# Comparative proteomic
# analysis of human lung telocytes with fibroblasts

**Yonghua Zheng** [a, #], **Dragos Cretoiu** [b, c, #], **Guoquan Yan** [d], **Sanda Maria Cretoiu** [b, e],
**Laurentiu M. Popescu** [b, f], **Xiangdong Wang** [g, *]

[a] *Department of Respirology, Xinhua Hospital Affiliated to Shanghai Jiao Tong University School of Medicine, Shanghai, China*
[b] *Division of Cellular and Molecular Medicine, Carol Davila University of Medicine and Pharmacy, Bucharest, Romania*
[c] *Department of Molecular Medicine, Victor Babeş National Institute of Pathology, Bucharest, Romania*
[d] *Department of Chemistry, Institute of Biomedical Sciences, Fudan University, Shanghai, China*
[e] *Department of Ultrastructural Pathology, Victor Babeş National Institute of Pathology, Bucharest, Romania*
[f] *Division of Advanced Studies, Victor Babeş National Institute of Pathology, Bucharest, Romania*
[g] *Department of Pulmonary Medicine and Biomedical Research Center, Zhongshan Hospital, Fudan University, Shanghai, China*

## Abstract

Telocytes (TCs) were recently described as interstitial cells with very long prolongations named telopodes (Tps; www.telocytes.com). Establishing the TC proteome is a priority to show that TCs are a distinct type of cells. Therefore, we examined the molecular aspects of lung TCs by comparison with fibroblasts (FBs). Proteins extracted from primary cultures of these cells were analysed by automated 2-dimensional nano-electrospray ionization liquid chromatography tandem mass spectrometry (2D Nano-ESI LC-MS/MS). Differentially expressed proteins were screened by two-sample $t$-test ($P < 0.05$) and fold change ($>2$), based on the bioinformatics analysis. We identified hundreds of proteins up- or down-regulated, respectively, in TCs as compared with FBs. TC proteins with known identities are localized in the cytoskeleton (87%) and plasma membrane (13%), while FB up-regulated proteins are in the cytoskeleton (75%) and destined to extracellular matrix (25%). These identified proteins were classified into different categories based on their molecular functions and biological processes. While the proteins identified in TCs are mainly involved in catalytic activity (43%) and as structural molecular activity (25%), the proteins in FBs are involved in catalytic activity (24%) and in structural molecular activity, particularly synthesis of collagen and other extracellular matrix components (25%). Anyway, our data show that TCs are completely different from FBs. In conclusion, we report here the first extensive identification of proteins from TCs using a quantitative proteomics approach. Protein expression profile shows many up-regulated proteins *e.g.* myosin-14, periplakin, suggesting that TCs might play specific roles in mechanical sensing and mechanochemical conversion task, tissue homoeostasis and remodelling/renewal. Furthermore, up-regulated proteins matching those found in extracellular vesicles emphasize TCs roles in intercellular signalling and stem cell niche modulation. The novel proteins identified in TCs will be an important resource for further proteomic research and it will possibly allow biomarker identification for TCs. It also creates the premises for understanding the pathogenesis of some lung diseases involving TCs.

**Keywords:** proteomics ● telocytes ● fibroblasts ● lung ● isobaric tags for relative and absolute quantification (iTRAQ) ● LC-MS/MS

## Introduction

Telocytes (TCs) are a novel defined cell type [1], resident in the stromal space of several mammalian and human organs [2–21], including in human lungs [22–24] (visit www.telocytes.com). TCs are characterized by very long and thin prolongations called telopodes (Tps) which suddenly emerge from a small cell body. Telopodes are tens to hundreds of micrometres long and have many dilations (podoms) interconnected by thin regions (podomeres) throughout their length [16]. The TCs interconnect with each other through point cell-to-cell contacts or gap junctions, forming a three-dimensional network [25, 26] and set up close contacts with other interstitial cells (*e.g.* macrophages, mast cells, lymphocytes) [12, 27]. Frequently, TCs could be observed in close vicinity with nerve cells, blood capillaries and stem

#These authors had equal contributions to this article.
*Correspondence to: Xiangdong WANG,
M.D., Ph.D., Department of Pulmonary Medicine and
Biomedical Research Center, Zhongshan Hospital,
Fudan University, Shanghai, China.
Tel.: +86-21-64041990-5420
Fax: +86-21-54961729
E-mail: xiangdong.wang@clintransmed.org

cell niches [28, 29]. Although the specific function(s) of TCs are still not established, it became increasingly clear that they have an integrative role, possibly for stem cells [7, 25, 30, 31], involving a long-distance communication confirmed by the presence of exosomes/ectosomes [16].

Telocytes were characterized ultrastructurally, immunophenotypically, electrophysiologically and their gene and microRNA profile were analysed [16, 31–35]. Telocytes are also involved in pathologies [5, 29, 36–41].

However, the protein expression profile for this type of cells has not been reported yet. In a previous study, we reported the gene expression profile of mice lung TCs compared to fibroblasts (FBs), and the results showed that more than ~1000 genes were found up- or down-regulated respectively [42]. Significantly improved technology in quantitative MS-based proteomics permits the measurement of relative protein loads in cell culture or tissue samples with unique precision [43, 44].

To prevent further confusion between TCs and other interstitial (stromal) cells, particularly with FBs and the so-called FBs-like cells, we carried out a comprehensive study using iTRAQ-coupled 2D LC-MS/MS analysis to identify and quantify the proteins. This study is the first that allows major insight into proteome differences between these cells in human lung and which identify the proteins that are specifically expressed in TCs.

# Material and methods

## Cell lines and tissue sampling

Human lung samples were obtained from the patients undergoing surgery for lung cancer. The normal tissue was defined as being located at a distance of at least 15 cm from the tumour tissue and verified by light microscopy. The application of human tissue for research was approved by the Ethical Evaluation Committee of Zhongshan Hospital, Fudan University, Shanghai, China. Human lung fibroblast cell lines were obtained from Chinese Academy of Science (Cat. no. GNHu28; Shanghai, China).

## Primary cell culture and lysis of lung TCs

The methods of isolation and culture of lung TCs were previously described by Zheng *et al.* [22]. Briefly, lung tissue was cut into small pieces and harvested under sterile conditions and collected into sterile tubes containing DMEM (Gibco, Grand Island, NY, USA), supplemented with 100 UI/ml penicillin and 0.1 mg/ml streptomycin (Sigma Chemical, St. Louis, MO, USA), and the samples were brought to the cell culture room immediately. Samples were further rinsed with sterile DMEM and minced into fragments about 1 mm$^3$, which were then incubated at 37°C for 4 hrs on an orbital shaker, with 1 mg/ml type II collagenase (Sigma-Aldrich, St. Louis, MO, USA) in PBS without Ca$^{2+}$ and Mg$^{2+}$. Dispersed cells were separated from non-digested tissue by the filtration through a 40-μm diameter cell strainer (BD Falcon, Franklin, NJ, USA), harvested by centrifugation and resuspended in DMEM supplemented with 10% foetal calf serum (Gibco), 100 UI/ml penicillin and

0.1 mg/ml streptomycin. Cell density was counted in a haemocytometer and viability was assessed using the Trypan blue. Cells were distributed in 25 cm$^2$ culture flasks at a density of $1 \times 10^5$ cells/cm$^2$ and maintained at 37°C in a humidified atmosphere (5% CO$_2$) until becoming semiconfluent (usually 4 days after plating). Culture medium was changed every 48 hrs. Cultured cells were examined by phase contrast microscope, under an inverted Olympus phase contrast microscope ($1 \times 51$). Cells ($1 \times 10^5$) were placed in 10-cm dishes with 10 ml high glucose DMEM (Gibco) complete medium, including 10% foetal calf serum (Gibco), 100 UI/ml penicillin and 0.1 mg/ml streptomycin (Sigma Chemical) in a humidified atmosphere of 5% CO$_2$ at 37°C. Confluent cells were trypsinized at day 5 and day 10 respectively. Approximately $10^6$ cells from day 5 or day 10 were resuspended in a solution of 9.5 moles/litre urea, 1% dithiothreitol (DTT), 40 mg/ml protease inhibitor cocktail, 0.2 mmoles/litre Na$_2$VO$_3$ and 1 mmole/litre NaF. The mixture was incubated and stirred by end-over-end rotation at 4°C for 60 min. The resultant suspension was centrifuged at 40,000 $\times$ g for 1 hr at 15°C. The supernatant was stored in small aliquots at −80°C, and the protein concentration was determined using a modified Bradford method.

## Automated 2-D nano-ESI LC-MS/MS analysis of peptides

Proteins extracted from primary cultures of TCs and FBs were analysed by automated 2-dimensional nano-electrospray ionization liquid
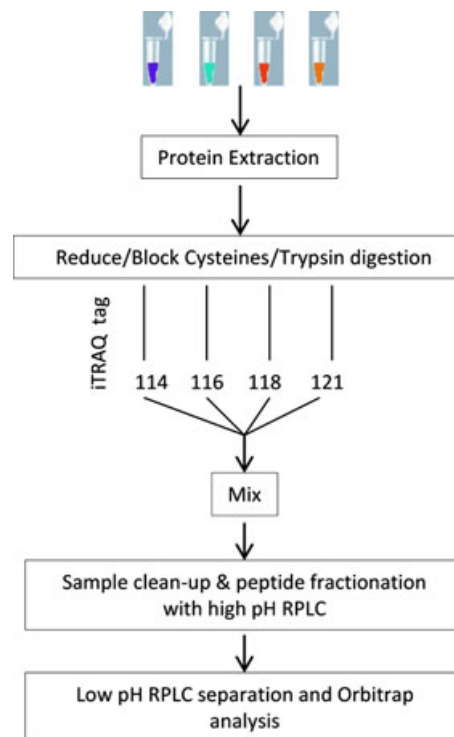


**Fig. 1** Proteomic process flow chart illustrating the steps involved in the differential analysis of TCs and FBs proteome in cell culture

**Table 1** Selected list of top 56 proteins identified with more than twofold change in TCs *versus* FBs at 5th day sorted by iTRAQ ratio and presenting the number of peptides hits

| Accession | Protein name | Peptides (95%) | %Cov (95) | iTRAQ ratio FBs:TCs | Fold enrichment in TCs | P |
|---|---|---|---|---|---|---|
| MYH14_HUMAN | Myosin-14 | 18 | 7.67 | 0.064 | 15.72 | 0.025 |
| SODM_HUMAN | Superoxide dismutase [Mn], mitochondrial | 10 | 35.14 | 0.104 | 9.6 | 0.000 |
| ALDH2_HUMAN | Aldehyde dehydrogenase, mitochondrial | 5 | 10.06 | 0.164 | 6.1 | 0.000 |
| PTGIS_HUMAN | Prostacyclin synthase | 7 | 15.80 | 0.199 | 5.03 | 0.005 |
| APOH_HUMAN | Beta-2-glycoprotein 1 | 2 | 4.35 | 0.210 | 4.75 | 0.041 |
| PPBT_HUMAN | Alkaline phosphatase, tissue-non-specific isozyme | 2 | 4.01 | 0.260 | 3.85 | 0.043 |
| PEPL_HUMAN | Periplakin | 4 | 2.85 | 0.284 | 3.52 | 0.032 |
| AL1B1_HUMAN | Aldehyde dehydrogenase X, mitochondrial | 5 | 13.93 | 0.313 | 3.2 | 0.024 |
| THIM_HUMAN | 3-ketoacyl-CoA thiolase, mitochondrial | 12 | 33.50 | 0.329 | 3.04 | 0.036 |
| KAD2_HUMAN | Adenylate kinase 2, mitochondrial | 8 | 41.42 | 0.336 | 2.97 | 0.001 |
| PLOD2_HUMAN | Procollagen-lysine, 2-oxoglutarate 5-dioxygenase 2 | 15 | 22.39 | 0.367 | 2.72 | 0.000 |
| AT1A1_HUMAN | Sodium/potassium-transporting ATPase subunit $\alpha$-1 | 17 | 18.77 | 0.375 | 2.67 | 0.000 |
| COX5B_HUMAN | Cytochrome c oxidase subunit 5B, mitochondrial | 4 | 34.11 | 0.380 | 2.63 | 0.006 |
| DNJC3_HUMAN | DnaJ homologue subfamily C member 3 | 2 | 3.77 | 0.392 | 2.55 | 0.024 |
| PRDX3_HUMAN | Thioredoxin-dependent peroxide reductase, mitochondrial | 6 | 23.83 | 0.395 | 2.53 | 0.028 |
| SUCA_HUMAN | Succinyl-CoA ligase [GDP-forming] subunit $\alpha$, mitochondrial | 5 | 17.63 | 0.399 | 2.51 | 0.008 |
| COX5A_HUMAN | Cytochrome c oxidase subunit 5A, mitochondrial | 6 | 58.67 | 0.408 | 2.45 | 0.000 |
| CH10_HUMAN | 10 kD heat shock protein, mitochondrial | 12 | 73.53 | 0.409 | 2.44 | 0.003 |
| CH60_HUMAN | 60 kD heat shock protein, mitochondrial | 60 | 62.30 | 0.414 | 2.42 | 0.003 |
| SQRD_HUMAN | Sulphide:quinone oxidoreductase, mitochondrial | 9 | 19.78 | 0.421 | 2.38 | 0.000 |
| ERP29_HUMAN | Endoplasmic reticulum resident protein 29 | 7 | 28.74 | 0.422 | 2.37 | 0.001 |
| K2C1_HUMAN | Keratin, type II cytoskeletal 1 | 12 | 15.06 | 0.435 | 2.3 | 0.004 |

**Table 1.** Continued

| Accession | Protein name | Peptides (95%) | %Cov (95) | iTRAQ ratio FBs:TCs | Fold enrichment in TCs | P |
|---|---|---|---|---|---|---|
| ERP44_HUMAN | Endoplasmic reticulum resident protein 44 | 4 | 8.13 | 0.442 | 2.26 | 0.002 |
| CATA_HUMAN | Catalase | 5 | 12.90 | 0.460 | 2.18 | 0.007 |
| ETFB_HUMAN | Electron transfer flavoprotein subunit β | 6 | 25.88 | 0.473 | 2.11 | 0.008 |
| SSBP_HUMAN | Single-stranded DNA-binding protein, mitochondrial | 6 | 50.68 | 0.476 | 2.1 | 0.028 |
| NLTP_HUMAN | Non-specific lipid-transfer protein | 9 | 12.43 | 0.477 | 2.1 | 0.010 |
| PDIA3_HUMAN | Protein disulphide-isomerase A3 | 45 | 52.48 | 0.480 | 2.08 | 0.019 |
| IDHP_HUMAN | Isocitrate dehydrogenase [NADP], mitochondrial | 5 | 9.29 | 0.492 | 2.03 | 0.000 |
| SPTB2_HUMAN | Spectrin β chain, brain 1 | 43 | 19.42 | 0.493 | 2.03 | 0.000 |
| RT36_HUMAN | 28S ribosomal protein S36, mitochondrial | 2 | 30.10 | 0.494 | 2.02 | 0.036 |

| Accession | Protein name | Peptides (95%) | %Cov (95) | iTRAQ ratio FBs:TCs | Fold enrichment in FBs | P |
|---|---|---|---|---|---|---|
| THIO_HUMAN | Thioredoxin | 5 | 51.43 | 2.006 | 2.01 | 0.008 |
| KPYM_HUMAN | Pyruvate kinase isozymes M1/M2 | 36 | 67.23 | 2.035 | 2.03 | 0.016 |
| CD166_HUMAN | CD166 antigen | 4 | 11.32 | 2.055 | 2.06 | 0.006 |
| WDR1_HUMAN | WD repeat-containing protein 1 | 10 | 18.15 | 2.061 | 2.06 | 0.001 |
| RS2_HUMAN | 40S ribosomal protein S2 | 10 | 31.06 | 2.088 | 2.09 | 0.000 |
| ACLY_HUMAN | ATP-citrate synthase | 11 | 11.08 | 2.089 | 2.09 | 0.000 |
| FLNC_HUMAN | Filamin-C | 73 | 32.40 | 2.160 | 2.16 | 0.000 |
| GSTO1_HUMAN | Glutathione S-transferase omega-1 | 2 | 9.54 | 2.181 | 2.18 | 0.028 |
| VAT1_HUMAN | Synaptic vesicle membrane protein VAT-1 homologue | 12 | 31.81 | 2.183 | 2.18 | 0.015 |
| CRTAP_HUMAN | Cartilage-associated protein | 2 | 3.74 | 2.273 | 2.27 | 0.049 |
| SYVC_HUMAN | Valyl-tRNA synthetase | 3 | 2.37 | 2.276 | 2.28 | 0.010 |
| VIME_HUMAN | Vimentin | 200 | 83.69 | 2.603 | 2.6 | 0.000 |
| 5NTD_HUMAN | 5′-nucleotidase | 6 | 14.81 | 2.603 | 2.6 | 0.000 |
| NEST_HUMAN | Nestin | 22 | 16.84 | 2.615 | 2.62 | 0.006 |
| PLIN3_HUMAN | Perilipin-3 | 9 | 26.50 | 2.625 | 2.63 | 0.000 |
| ANXA6_HUMAN | Annexin A6 | 21 | 31.35 | 2.714 | 2.71 | 0.005 |
| SERA_HUMAN | D-3-phosphoglycerate dehydrogenase | 4 | 8.07 | 2.773 | 2.77 | 0.017 |

© 2014 The Authors.                                                                                      571

Journal of Cellular and Molecular Medicine published by John Wiley & Sons Ltd and Foundation for Cellular and Molecular Medicine.

**Table 1.** Continued

| Accession | Protein name | Peptides (95%) | %Cov (95) | iTRAQ ratio FBs:TCs | Fold enrichment in FBs | P |
|---|---|---|---|---|---|---|
| G3P_HUMAN | Glyceraldehyde-3-phosphate dehydrogenase | 42 | 64.48 | 2.819 | 2.82 | 0.001 |
| S10AD_HUMAN | Protein S100-A13 | 5 | 44.90 | 2.823 | 2.82 | 0.000 |
| RL15_HUMAN | 60S ribosomal protein L15 | 2 | 7.84 | 3.130 | 3.13 | 0.006 |
| LEG1_HUMAN | Galectin-1 | 27 | 91.11 | 3.133 | 3.13 | 0.000 |
| GDIR1_HUMAN | Rho GDP-dissociation inhibitor 1 | 4 | 18.14 | 3.241 | 3.24 | 0.001 |
| FSCN1_HUMAN | Fascin | 6 | 16.63 | 3.255 | 3.25 | 0.004 |
| SCRN1_HUMAN | Secernin-1 | 2 | 5.80 | 3.734 | 3.73 | 0.019 |
| CO6A3_HUMAN | Collagen α-3(VI) chain | 41 | 16.53 | 4.707 | 4.71 | 0.000 |

**Table 2** Selected list of top 56 proteins identified with more than twofold change in TCs *versus* FBs at 10th day sorted by iTRAQ ratio and presenting the number of petides hits

| Accession | Protein name | Peptides (95%) | %Cov (95) | iTRAQ ratio FBs:TCs | Fold enrichment in TCs | P |
|---|---|---|---|---|---|---|
| SODM_HUMAN | Superoxide dismutase [Mn], mitochondrial | 10 | 35.14 | 0.120 | 8.36 | 0.001 |
| PTGIS_HUMAN | Prostacyclin synthase | 7 | 15.8 | 0.123 | 8.12 | 0.001 |
| MYH14_HUMAN | Myosin-14 | 18 | 7.669 | 0.144 | 6.96 | 0.036 |
| PLOD2_HUMAN | Procollagen-lysine,2-oxoglutarate 5-dioxygenase 2 | 15 | 22.39 | 0.211 | 4.74 | 0.000 |
| ANXA3_HUMAN | Annexin A3 | 3 | 12.69 | 0.231 | 4.32 | 0.027 |
| ICAM1_HUMAN | Intercellular adhesion molecule 1 | 6 | 14.66 | 0.267 | 3.75 | 0.001 |
| NAMPT_HUMAN | Nicotinamide phosphoribosyltransferase | 3 | 5.906 | 0.325 | 3.08 | 0.005 |
| CYB5_HUMAN | Cytochrome b5 | 4 | 32.09 | 0.333 | 3 | 0.004 |
| EZRI_HUMAN | Ezrin | 19 | 31.4 | 0.352 | 2.84 | 0.002 |
| MYH10_HUMAN | Myosin-10 | 45 | 19.59 | 0.419 | 2.38 | 0.007 |
| FLNB_HUMAN | Filamin-B | 96 | 41.78 | 0.430 | 2.33 | 0.000 |
| THIM_HUMAN | 3-ketoacyl-CoA thiolase, mitochondrial | 12 | 33.5 | 0.434 | 2.3 | 0.000 |
| SQRD_HUMAN | Sulphide:quinone oxidoreductase, mitochondrial | 9 | 19.78 | 0.435 | 2.3 | 0.000 |
| PLAK_HUMAN | Junction plakoglobin | 3 | 4.564 | 0.447 | 2.24 | 0.011 |
| DHB4_HUMAN | Peroxisomal multifunctional enzyme type 2 | 11 | 25 | 0.456 | 2.19 | 0.030 |
| KAD2_HUMAN | Adenylate kinase 2, mitochondrial | 8 | 41.42 | 0.484 | 2.07 | 0.000 |

**Table 2.** Continued

| Accession | Protein name | Peptides (95%) | %Cov (95) | iTRAQ ratio FBs:TCs | Fold enrichment in FBs | P |
|---|---|---|---|---|---|---|
| TAGL_HUMAN | Transgelin | 15 | 75.12 | 1.996 | 2 | 0.000 |
| EHD2_HUMAN | EH domain-containing protein 2 | 8 | 17.13 | 2.021 | 2.02 | 0.000 |
| RL18A_HUMAN | 60S ribosomal protein L18a | 3 | 17.61 | 2.022 | 2.02 | 0.002 |
| RL13A_HUMAN | 60S ribosomal protein L13a | 2 | 6.897 | 2.023 | 2.02 | 0.003 |
| PTRF_HUMAN | Polymerase I and transcript release factor | 17 | 42.82 | 2.024 | 2.02 | 0.036 |
| VINC_HUMAN | Vinculin | 38 | 36.95 | 2.027 | 2.03 | 0.000 |
| KPYM_HUMAN | Pyruvate kinase isozymes M1/M2 | 36 | 67.23 | 2.054 | 2.05 | 0.004 |
| GSTO1_HUMAN | Glutathione S-transferase omega-1 | 2 | 9.544 | 2.059 | 2.06 | 0.008 |
| LASP1_HUMAN | LIM and SH3 domain protein 1 | 6 | 22.61 | 2.068 | 2.07 | 0.000 |
| THIO_HUMAN | Thioredoxin | 5 | 51.43 | 2.072 | 2.07 | 0.017 |
| CSRP1_HUMAN | Cysteine and glycine-rich protein 1 | 3 | 21.76 | 2.105 | 2.11 | 0.003 |
| GDIR1_HUMAN | Rho GDP-dissociation inhibitor 1 | 4 | 18.14 | 2.121 | 2.12 | 0.024 |
| CNN2_HUMAN | Calponin-2 | 9 | 37.86 | 2.131 | 2.13 | 0.000 |
| SEPT9_HUMAN | Septin-9 | 3 | 5.119 | 2.158 | 2.16 | 0.010 |
| PROF1_HUMAN | Profilin-1 | 23 | 75.71 | 2.176 | 2.18 | 0.000 |
| CO1A2_HUMAN | Collagen $\alpha$-2(I) chain | 9 | 7.906 | 2.202 | 2.2 | 0.012 |
| CD166_HUMAN | CD166 antigen | 4 | 11.32 | 2.203 | 2.2 | 0.009 |
| CD44_HUMAN | CD44 antigen | 7 | 9.569 | 2.251 | 2.25 | 0.012 |
| RL24_HUMAN | 60S ribosomal protein L24 | 6 | 31.21 | 2.256 | 2.26 | 0.002 |
| STMN1_HUMAN | Stathmin | 6 | 32.21 | 2.303 | 2.3 | 0.003 |
| 5NTD_HUMAN | 5′-nucleotidase | 6 | 14.81 | 2.309 | 2.31 | 0.007 |
| G3P_HUMAN | Glyceraldehyde-3-phosphate dehydrogenase | 42 | 64.48 | 2.349 | 2.35 | 0.000 |
| ANXA5_HUMAN | Annexin A5 | 30 | 54.37 | 2.409 | 2.41 | 0.003 |
| FSCN1_HUMAN | Fascin | 6 | 16.63 | 2.467 | 2.47 | 0.001 |
| LEG1_HUMAN | Galectin-1 | 27 | 91.11 | 2.472 | 2.47 | 0.000 |
| PLIN3_HUMAN | Perilipin-3 | 9 | 26.5 | 2.568 | 2.57 | 0.000 |
| A2MG_HUMAN | $\alpha$-2-macroglobulin | 7 | 4.342 | 2.606 | 2.61 | 0.027 |
| H15_HUMAN | Histone H1.5 | 7 | 23.45 | 2.692 | 2.69 | 0.009 |
| MAP1B_HUMAN | Microtubule-associated protein 1B | 11 | 5.146 | 2.700 | 2.7 | 0.036 |

**Table 2.** Continued

| Accession | Protein name | Peptides (95%) | %Cov (95) | iTRAQ ratio FBs:TCs | Fold enrichment in FBs | P |
|---|---|---|---|---|---|---|
| VAT1_HUMAN | Synaptic vesicle membrane protein VAT-1 homologue | 12 | 31.81 | 2.717 | 2.72 | 0.000 |
| LEG3_HUMAN | Galectin-3 | 10 | 30.4 | 2.800 | 2.8 | 0.000 |
| MFGM_HUMAN | Lactadherin | 6 | 17.05 | 2.844 | 2.84 | 0.019 |
| VIME_HUMAN | Vimentin | 200 | 83.69 | 2.848 | 2.85 | 0.000 |
| NEST_HUMAN | Nestin | 22 | 16.84 | 2.865 | 2.87 | 0.007 |
| NQO1_HUMAN NAD(P) | H dehydrogenase [quinone] 1 | 2 | 7.664 | 2.874 | 2.87 | 0.006 |
| H12_HUMAN | Histone H1.2 | 7 | 30.99 | 3.039 | 3.04 | 0.001 |
| CSRP2_HUMAN | Cysteine and glycine-rich protein 2 | 1 | 7.772 | 3.135 | 3.14 | 0.022 |
| SH3L3_HUMAN | SH3 domain-binding glutamic acid-rich-like protein 3 | 3 | 34.41 | 3.252 | 3.25 | 0.007 |
| CO6A3_HUMAN | Collagen α-3(VI) chain | 41 | 16.53 | 4.428 | 4.43 | 0.000 |
| MARE1_HUMAN | Microtubule-associated protein RP/EB family member 1 | 2 | 7.463 | 89.966 | 89.97 | 0.018 |

chromatography tandem mass spectrometry as was previously described by Wang *et al.* [45] and Jin *et al.*[46].

## Sample preparation

The samples were ground in liquid nitrogen. One millilitre of lysis buffer (8 M urea, 1× Protease Inhibitor Cocktail; Roche Ltd., Basel, Switzerland) was added to sample, followed by sonication on ice and centrifugation at 29,000 × g. for 10 min. at 4°C. The supernatant was transferred to a fresh tube and stored at −80°C until needed.

## iTRAQ labelling and protein digestion

For each sample, proteins were precipitated with ice-cold acetone and then were redissolved in the dissolution buffer (0.5 M triethylammonium bicarbonate, 0.1% SDS). Then proteins were quantified by the bicinchoninic acid protein assay, and 100 μg of protein was tryptically digested and the resultant peptide mixture was labelled using chemicals from the iTRAQ reagent kit (Applied Biosystems, Foster City, CA, USA). Disulphide bonds were reduced in 5 mM Tris-(2-carboxyethy) phosphine (TCEP) for 1 hr at 60°C, followed by blocking cysteine residues in 10 mM methyl methanethiosulfonate (MMTS) for 30 min. at room temperature, before digestion with sequence-grade modified trypsin (Promega, Madison, WI, USA). For labelling, each iTRAQ reagent was dissolved in 50 μl of isopropanol and added to the respective peptide mixture.

Proteins were labelled with the iTRAQ tags as follows: Fibroblast (5 days) − 114 isobaric tag, TCs (5 days) − 116 isobaric tag, Fibroblast (10 days) − 118 isobaric tag, TCs (10 days) − 121 isobaric tag. The labelled samples were combined and dried in vacuo. A SepPac™ C18 cartridge (1 cm³/50 mg, Waters Corporation, Milford, MA, USA) was used to remove the salt buffer and then was dried in a vacuum concentrator for the next step.

## High pH reverse phase separation

The peptide mixture was redissolved in the buffer A (buffer A: 20 mM ammonium formate in water, pH 10.0, adjusted with ammonium hydroxide), and then fractionated by high pH separation using a Aquity UPLC system (Waters Corporation) connected to a reverse phase column (XBridge C18 column, 2.1 × 150 mm, 3.5 μm, 300 Å, Waters Corporation). High pH separation was performed with a linear gradient. Starting from 2% B to 40% B in 45 min. (B: 20 mM ammonium formate in 90% ACN, pH 10.0, adjusted with ammonium hydroxide). The column was re-equilibrated at initial conditions for 15 min. The column flow rate was maintained at 200 μl/min. and column temperature was maintained at room temperature [47]. Fourteen fractions were collected, and each fraction was dried in a vacuum concentrator for the next step.

## Low pH nano-HPLC-MS/MS analysis

The peptides were resuspended with 80 μl solvent C (C: water with 0.1% formic acid; D: ACN with 0.1% formic acid), separated by nanoLC and analysed by on-line electrospray tandem mass spectrometry. The experiments were performed on a Nano Aquity UPLC system (Waters Corporation) connected to an LTQ Orbitrap XL mass spectrometer (Thermo Electron Corp., Bremen, Germany) equipped with an online nanoelectrospray ion source (Michrom Bioresources, Auburn, CA, USA). 20 μl peptide sample was loaded onto the Thermo Scientific Acclaim PepMap C18 column (100 μm × 2 cm, 3 μm particle size), with a flow of 10 μl/min. for 5 min. and subsequently separated on the analytical column (Acclaim PepMap C18, 75 μm × 15 cm) with a linear gradient, from 5% D to 45%
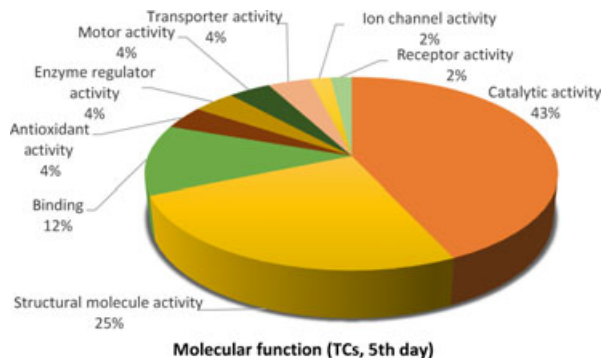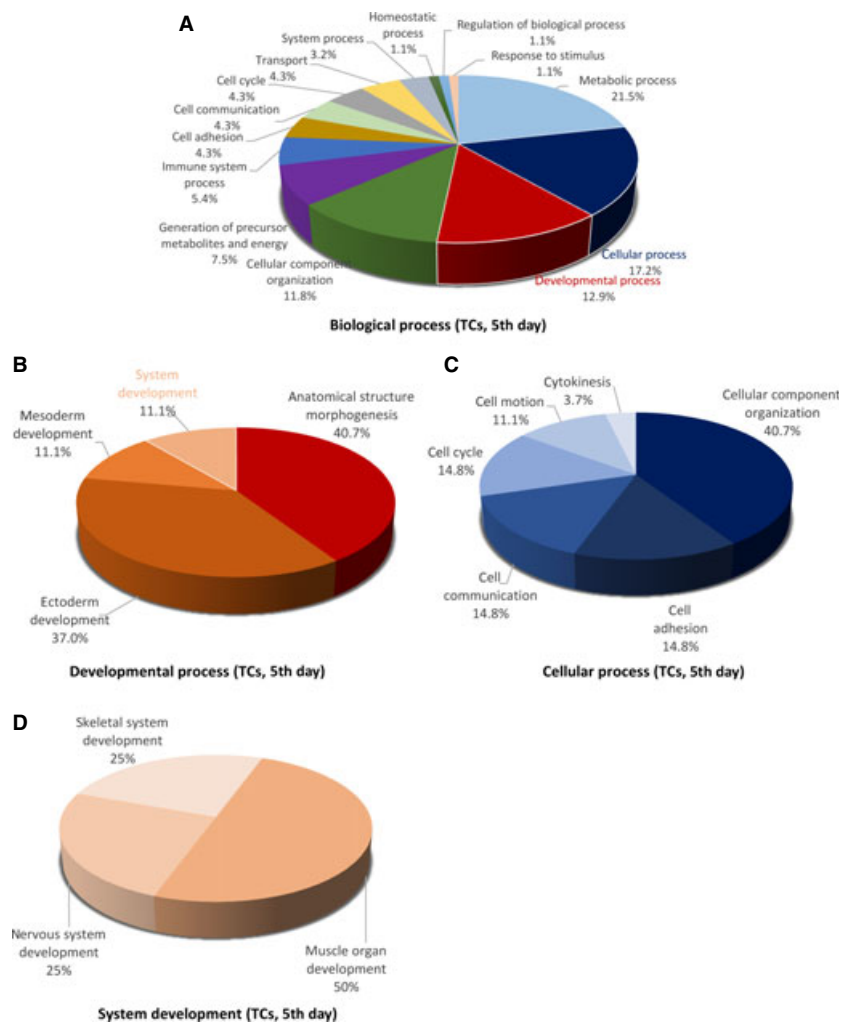
**Fig. 2** Pie chart representation of the distribution of identified proteins in TCs (cell culture, 5th day) according to their molecular functions. Categorizations were based on information provided by the online resource PANTHER classification system.
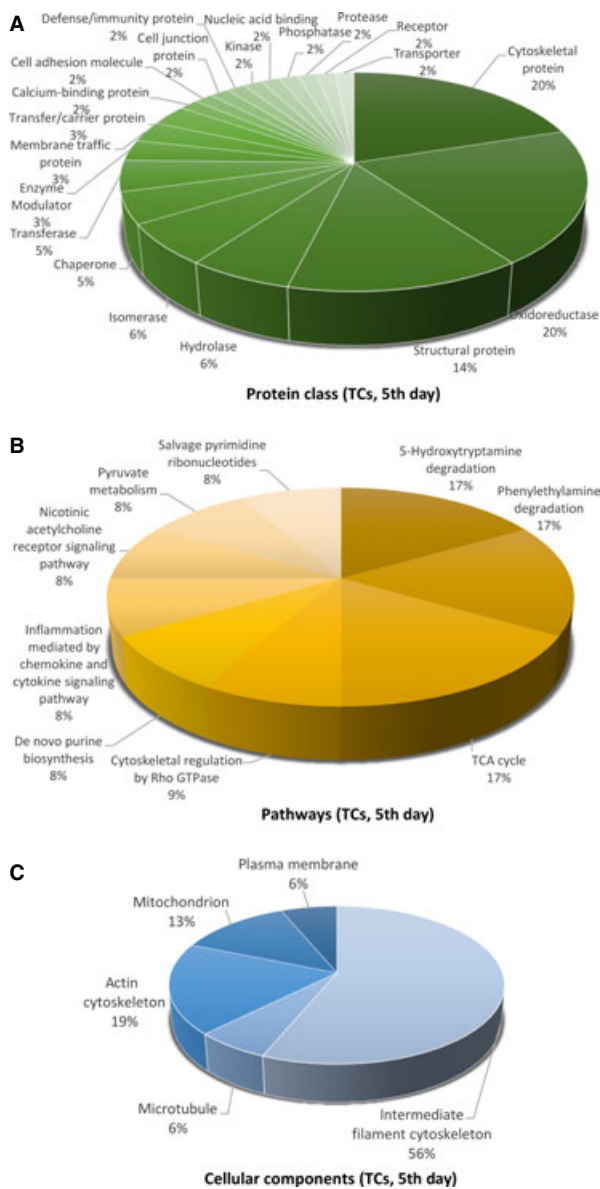
D in 165 min. The column was re-equilibrated at initial conditions for 15 min. The column flow rate was maintained at 300 nl/min. and column temperature was maintained at 35°C. The electrospray voltage of 1.9 kV *versus* the inlet of the mass spectrometer was used.

LTQ Orbitrap XL mass spectrometer was operated in the data-dependent mode to switch automatically between MS and MS/MS acquisition. Survey full-scan MS spectra (m/z 400-1600) were acquired in the Orbitrap with a mass resolution of 30,000 at m/z 400, followed by five sequential HCD-MS/MS scans. The automatic gain control was set to 500,000 ions to prevent over-filling of the ion trap. The minimum MS signal for triggering MS/MS was set to 1000. In all cases, one microscan was recorded. MS/MS scans were acquired in the Orbitrap with a mass resolution of 7500. The dissociation mode was HCD (higher energy C-trap dissociation). Dynamic exclusion was used with two repeat counts, 10-sec. repeat duration, and the m/z values triggering MS/MS were put on an exclusion list for 120 sec. For MS/MS, precursor ions were activated using 40% normalized collision energy and an activation time of 30 ms.



**Fig. 3** Pie chart representation of the distribution of identified proteins in TCs (cell culture, 5th day) according to their biological processes (**A**), cellular processes (**B**), developmental processes (**C**) and system development (**D**) involvement.

© 2014 The Authors.

Journal of Cellular and Molecular Medicine published by John Wiley & Sons Ltd and Foundation for Cellular and Molecular Medicine.

575

**Fig. 4** Pie chart representation of the distribution of identified proteins in TCs (cell culture, 5th day) according to their protein class (**A**), pathways (**B**) and cellular components (**C**) classifications.

## Database searching, criteria and protein parameterization

Protein identification and quantification for the iTRAQ experiment was performed with the ProteinPilot software version 4.0 (Applied Biosystems). The database was the Human UniProtKB/Swiss-Prot database (Release 2011_10_15, with 20248 sequences). The Paragon Algorithm in ProteinPilot software was used for peptide identification and isoform-specific quantification. The data search parameters were set up as follows: trypsin (KR) cleavage with two missed cleavage was consid-

ered; fixed modification in cysteines by MMTS; iTRAQ modification in peptide N termini, methionine oxidation and iTRAQ modification in lysine residues were set as variable modification. To minimize false positive results, a strict cut-off for protein identification was applied with the unused ProtScore ≥1.3, which corresponds to a confidence limit of 95%, and at least two peptides with the 95% confidence were considered for protein quantification. The resulting data set was auto bias corrected to get rid of any variations imparted because of unequal mixing during combining different labelled samples. For iTRAQ quantification, the peptide for quantification was automatically selected by Pro Group algorithm (at least two peptides with 99% confidence) to calculate the reporter peak area, error factor and p-value. For the selection of differentially expressed proteins, we considered the following situation: (*i*) the proteins must contain at least two unique high-scoring peptides; (*ii*) the proteins must have a $P < 0.05$ and the proteins identified with mass tag changes ratio must be ≥1.3 or ≤0.75.

Differentially expressed proteins were screened by two-sample *t*-test ($P < 0.05$) and fold change (>2), based on the bioinformatics analysis.

## Data set analysis

MS/MS fragmentation spectra were analysed using PEAKS search engine tool (PEAKS Studio 7; Bioinformatics Solutions Inc., Waterloo, ON, Canada).

The protein details obtained were analysed for the function, process, location, by PANTHER (Protein ANalysis THrough Evolutionary Relationships) classification system (http://www.pantherdb.org/) [48] which is based on a controlled dialect to describe a protein regarding its subcellular localization, molecular function or biological process.

Top over-expressed proteins were used to create radar (spider) plots Using Microsoft Excel.

# Results

This study utilizes a novel proteomic approach based on isobaric tags for relative and absolute quantification (iTRAQ) using nano liquid chromatography tandem mass spectrometry analysis to identify spe-
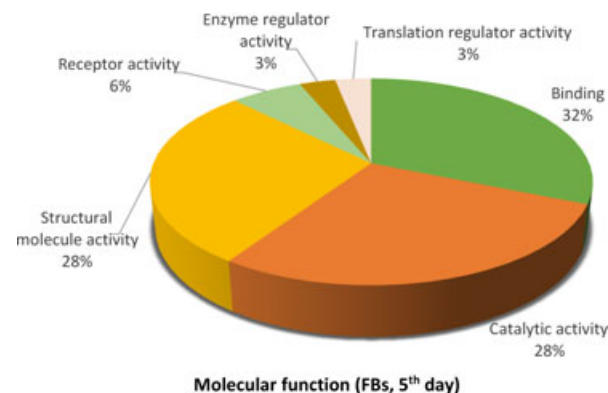


**Fig. 5** Pie chart representation of the distribution of identified proteins in FBs (cell culture, 5th day) according to their molecular functions. Categorizations were based on information provided by the online resource PANTHER classification system.

cifically over expressed proteins in TCs comparative to FBs. Figure 1 shows the sequence of connected procedural steps used in this protocol.

We identified a total of 1609 proteins by iTRAQ technology using nano LC-MS/MS analysis. The temporal proteome was evaluated at 5 and 10 days, respectively, and the selected lists of differentially up-regulated proteins identified in TCs and FBs, in cell culture, are shown in Table 1 (5th day) and Table 2 (10th day).

## TCs *versus* FBs, 5th day in cell culture

### Identification of the differentially expressed protein

We found that in TCs, as compared to FBs, there are 39 up-regulated proteins, especially Myosin-14 (15.72-fold). We subsequently examined the FBs by comparison with TCs and found that there are 25 up-regulated proteins, especially collagen alfa 3(VI) chain (4.71-fold), secernin-1 (3.73-fold), fascin (3.25-fold) as detailed in Tables S1 and S2.

### Bioinformatic analyses of the identified proteins

The distributions of differentially abundant proteins in putative functional categories are shown in Figures 2–7 according to the PANTHER. The various *molecular functions* which were found to be mapped with the participation of the identified proteins in TCs are involved mainly in catalytic activity (43%) and as structural molecule activity (25%; Fig. 2) compared with FBs in which they are chiefly involved in binding (32%), catalytic activity (28%) and as structural molecule activity (28%; Fig. 5).

The 39 proteins identified in TCs were assigned to following main *biological processes*: metabolic process (21.5%), cellular process (17.2%), developmental process (12.9%) and cellular component organization (11.8%), generation of precursor metabolites and energy (7.5%) immune system process (5.4%), cell communication, transport, cell adhesion, cell cycle (each 4.3%), system process (3.2%), homoeostatic process, regulation of biological process, response to stimulus (each 1.1%; Fig. 3A). The 25 proteins over expressed in FBs were assigned dominantly to metabolic process (21.4%), cellular pro-
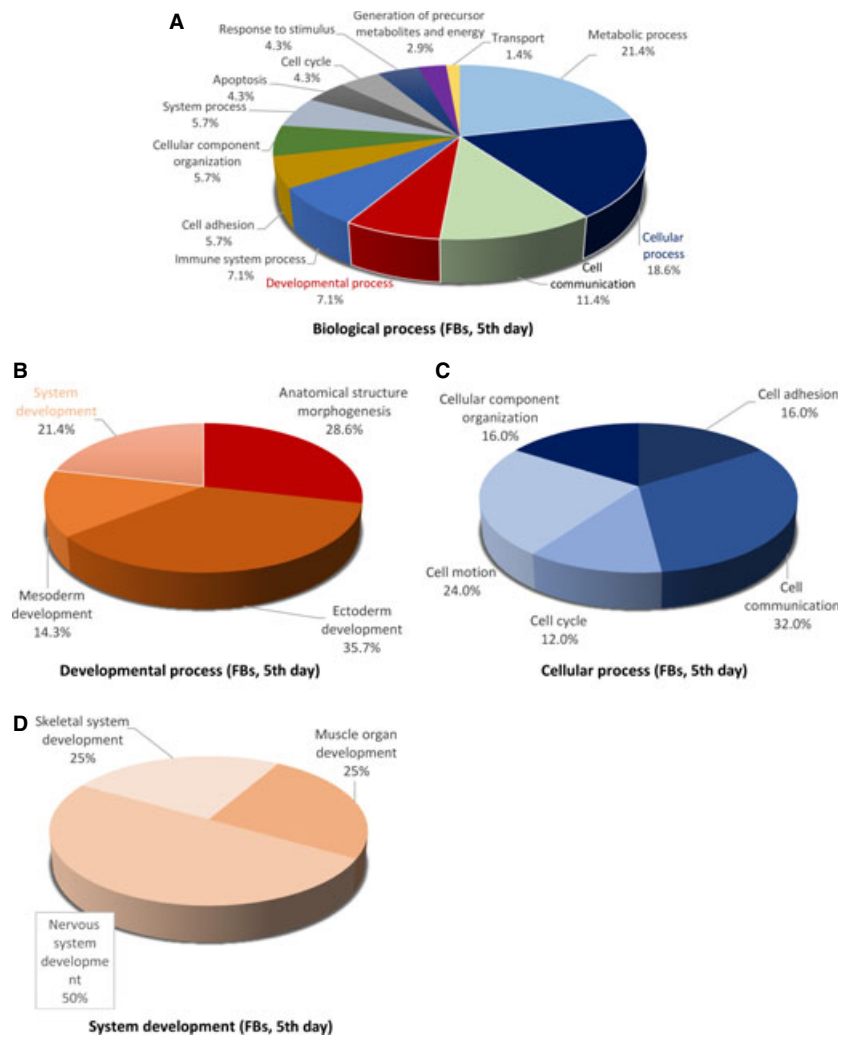
**Fig. 6** Pie chart representation of the distribution of identified proteins in FBs (cell culture, 5th day) according to their biological processes (**A**), cellular processes (**B**), developmental processes (**C**) and system development (**D**) involvement.

cess (18.6%), cell communication (11.4%), developmental and immune system processes (each 7.1%) and cell adhesion (5.7%; Fig. 6A).

The main *developmental processes* which engage TCs proteins are anatomical structure morphogenesis (~41%), ectoderm development (37%), mesoderm development and system development (each ~11%; Fig. 3B), comparative to FBs where proteins are engaged in anatomical structure morphogenesis (~29%), ectoderm development (35.7%), mesoderm development (14.3%) and system development (21.4%) respectively (Fig. 6B).

The *cellular processes* which involve TCs proteins are cellular component organization (~41%), cell communication, cell adhesion and cell cycle (each ~15%; Fig. 3C), while FBs proteins are involved in cell communication (32%), cell motion (24%), cell adhesion and cellular component organization (each 16%) and cell cycle (12%; Fig. 6C).

There is a big difference regarding *system development functions* between TCs and FBs: muscle organ development 50%, nervous system and skeletal muscle development 25% each in TCs (Fig. 3D) and 50% nervous system development and skeletal muscle and muscle organ development 25% each for FBs (Fig. 6D).

The proteins in TCs are attributed to the following *protein classes*: cytoscheletal proteins (20%), oxidoreductase (20%) and structural proteins (14%; Fig. 4A), hydrolase and isomerase (each 6%), chaperone and transferase (each 5%), while in FBs proteins pertain to cytoscheletal proteins (14%), oxidoreductase (11%), signalling molecule (9%), calcium-binding protein, cell adhesion molecule, nucleic acid binding, structural proteins and transferase (each 7%; Fig. 7A).

The different highly significant *pathway* map associated with the proteins in TCs showed that they are involved in 5-HT degradation (17%), TCA cycle (17%) and phenyletylamine degradation (17%) and cytoskeletal regulation by Rho GTPase (9%) and *de novo* purine shynthesis (8%; Fig. 4B). By comparison, FBs proteome clearly depicts that they are involved in glycolysis (15%), Huntington disease (15%), integrin signalling pathway (14%), pyruvate metabolism and (14%; Fig. 7B).

The *cellular localization* of TCs proteome demonstrated proteins from intermediate filaments (56%), actin cytoscheleton (19%), mitochondria (13%), microtubule (6%) and plasma membrane (6%; Fig. 4C). In FBs, 75% of the proteins belong to the cytoskeleton and 25% are destined to the extracellular matrix (Fig. 7C).

Figure 8 represents the heat map based on the results of protein quantification and demonstrates that proteins are differentially expressed between TCs and FBs.

## TCs *versus* FBs, 10th day in cell culture

### Identification of the differentially expressed protein

We discovered that in TCs, as compared to FBs, there are 24 up-regulated proteins, especially superoxide dismutase (8.36-fold) and prostacyclin synthase 6A (8.12-fold). Myosin-14 remains up-

regulated at 10 days (6.6-fold). In FBs, there are 40 up-regulated proteins especially Microtubule-associated protein RP/EB family member 1 (89.96-fold) and Collagen α-3(VI) chain (4.428-fold) comparative to TCs (Tables S3 and S4).

### Bioinformatic analyses of the identified proteins

Figures 9–14 show the distribution of proteins in presumed functional categories according to the PANTHER. The various *molecular functions* which were attributed of the identified proteins in TCs are
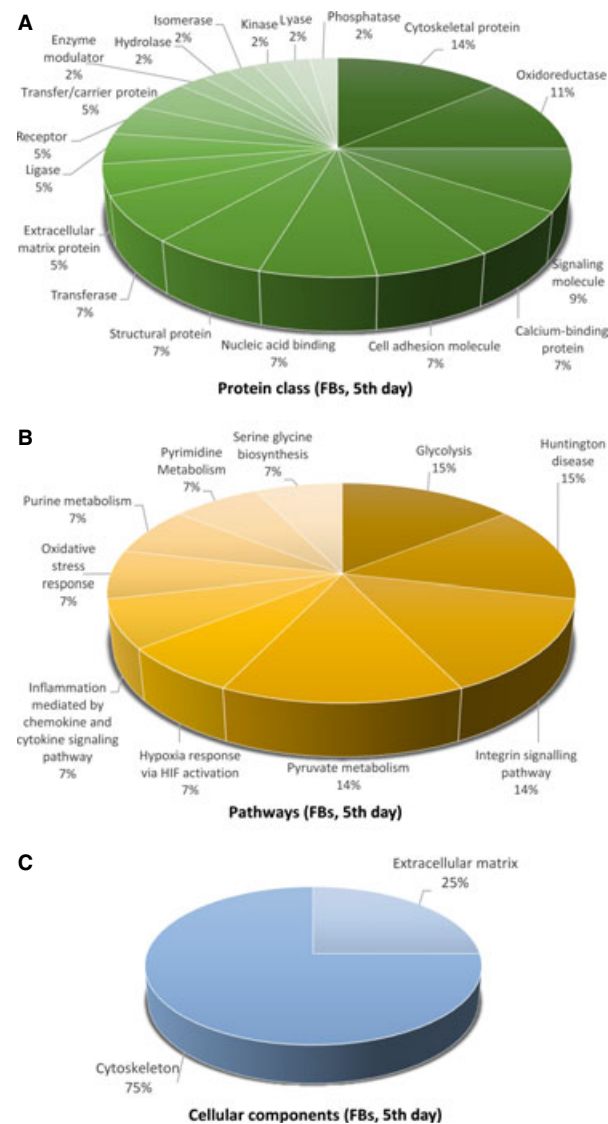
**Fig. 7** Pie chart representation of the distribution of identified proteins in FBs (cell culture, 5th day) according to their protein class (**A**), pathways (**B**) and cellular components (**C**) classifications.
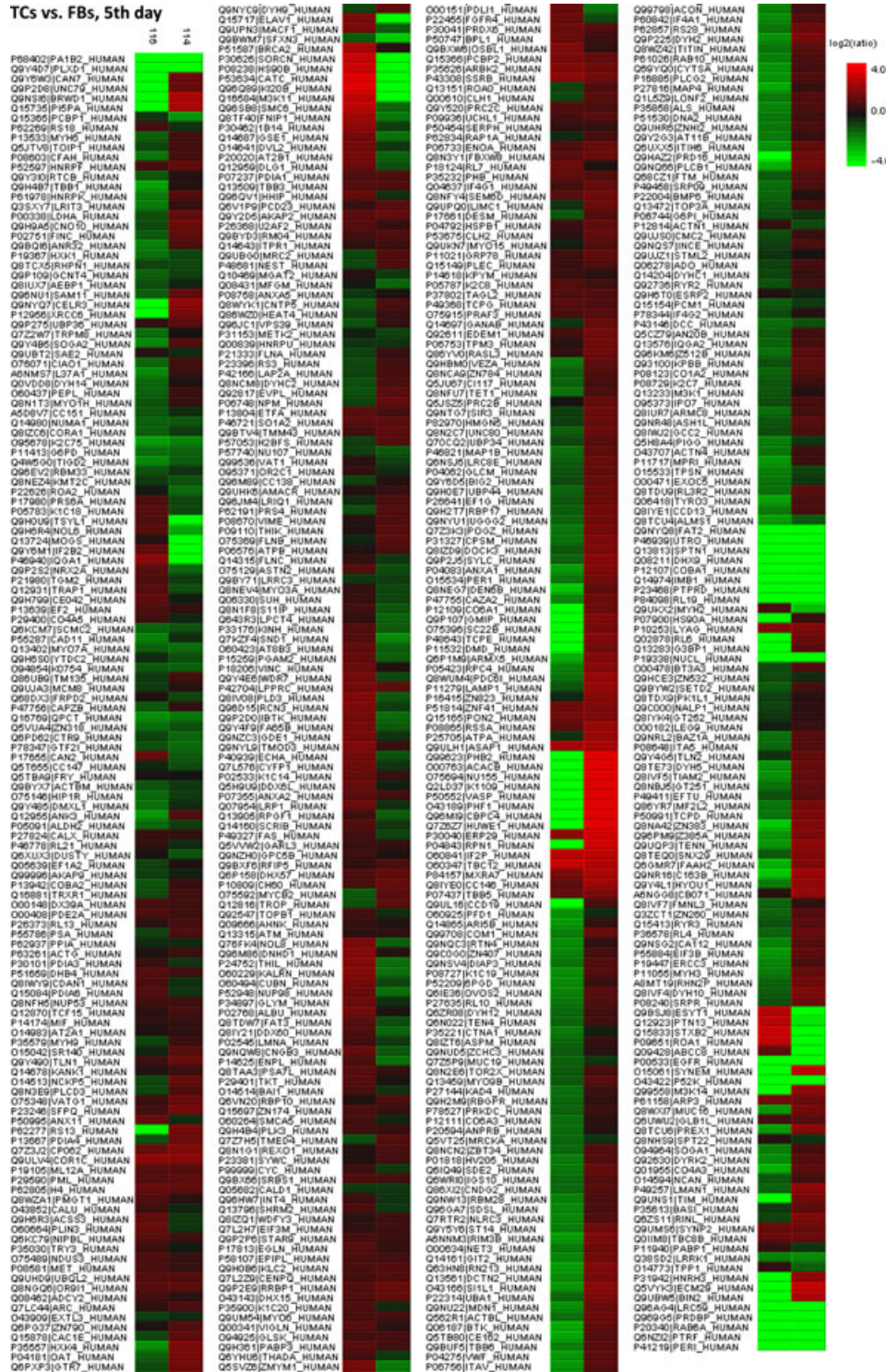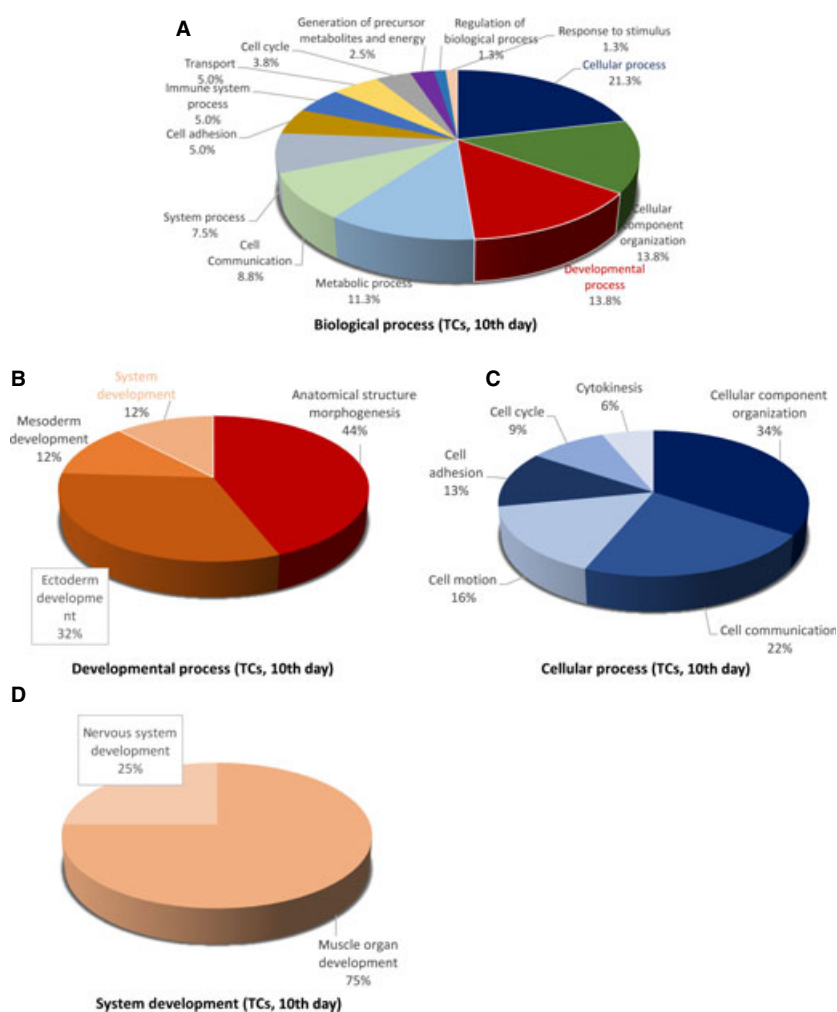
**Fig. 8** Heat map depicting significance results between TCs and FBs (cell culture, 5th day). Experimental samples are clustered on the horizontal axis and protein spots on the vertical axis. Red indicates increased and green decreased expression ratio, while black squares indicate no change in protein abundance. The colour gradient indicates the magnitude of fold change.

involved mainly in structural molecule activity (38%), in catalytic activity (24%) and binding (22%; Fig. 9) compared with FBs where are mostly implicated in binding (36%), structural molecule activity (29%), catalytic activity (13%; Fig. 12).

The 39 proteins identified in TCs were assigned to following main *biological processes*: cellular process (21.3%), developmental process (13.8%), cellular component organization (13.8%) and metabolic process (11.3%), cell–cell communication (8.8%), system processes (7.5%) cell adhesion (5%), immune system process (5%), transport (5%), generation of precursor metabolites and energy (2.5%), cell cycle (3.8%), regulation of biological process, response to stimulus (each 1.3%; Fig. 10A). The 25 proteins over expressed in FBs were assigned dominantly to cellular process (19.2%), metabolic processes (13.3%), cell communication (10.8%), developmental processes (10%), immune system process (9.2%), cellular component organization (7.5%), cell adhesion (6.7%), system process (6.7%), response to stimulus (5%) apoptosis and transport 3.3% each (Fig. 13A).
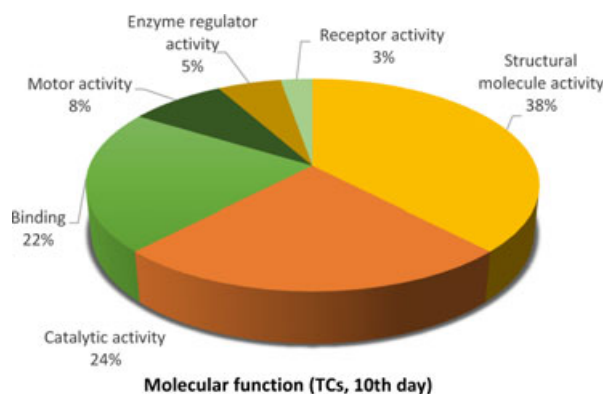


**Fig. 9** Pie chart representation of the distribution of identified proteins in TCs (cell culture, 10th day) according to their molecular functions. Categorizations were based on information provided by the online resource PANTHER classification system.
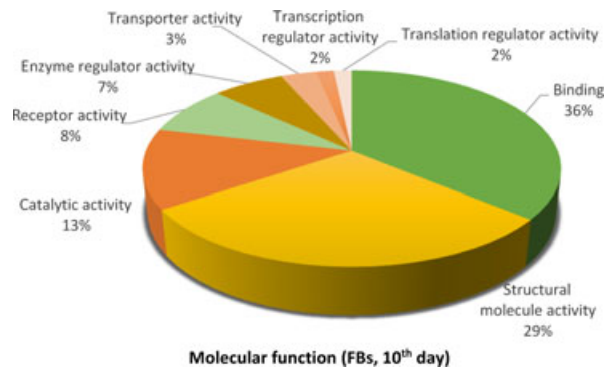


**Fig. 10** Pie chart representation of the distribution of identified proteins in TCs (cell culture, 10th day) according to their biological processes (**A**), cellular processes (**B**), developmental processes (**C**) and system development (**D**) involvement.

**A**



**Protein class (TCs, 10th day)**

**B**



**Pathways (TCs, 10th day)**

**C**



**Cellular components (TCs, 10th day)**

**Fig. 11** Pie chart representation of the distribution of identified proteins in TCs (cell culture, 10th day) according to their protein class (**A**), pathways (**B**), and cellular components (**C**) classifications.



**Molecular function (FBs, 10th day)**

**Fig. 12** Pie chart representation of the distribution of identified proteins in FBs (cell culture, 10th day) according to their molecular functions. Categorizations were based on information provided by the online resource PANTHER classification system.

motion (16%) and cell adhesion (13%; Fig. 10C), while FBs proteins are involved in cell communication (34.2%), cellular component organization (~24%), cell adhesion (~21%), cell motion (10%; Fig. 13C).
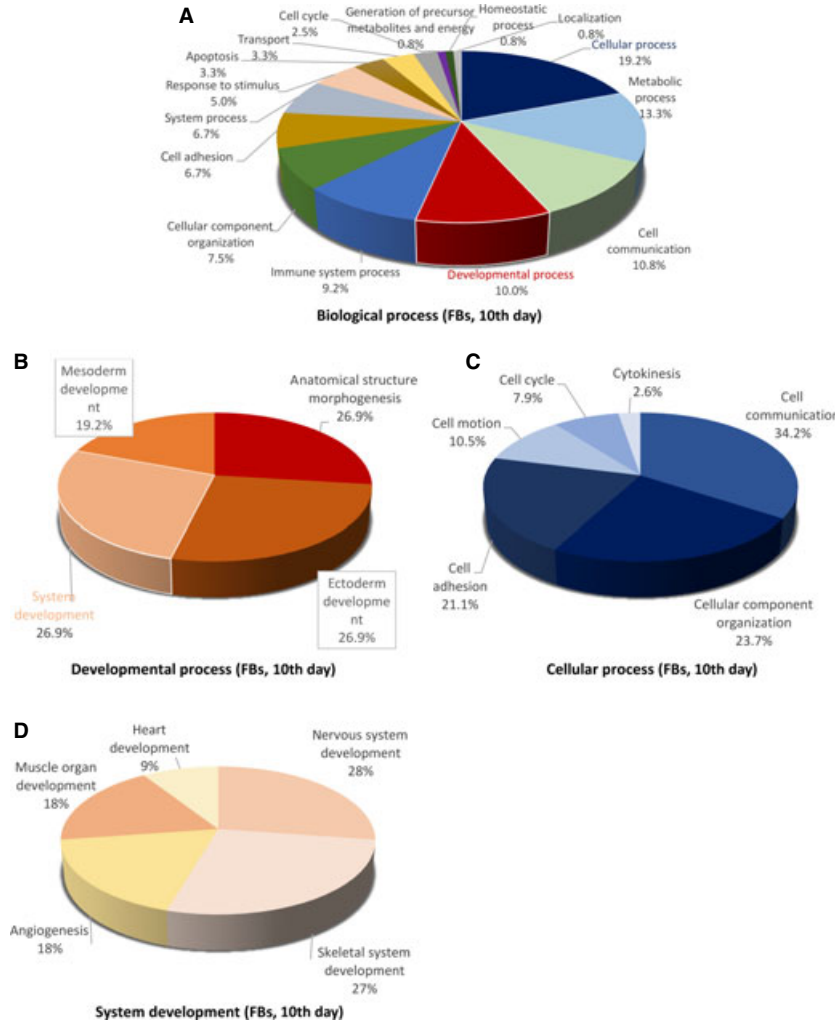
There is a big difference regarding *system development functions* between TCs and FBs: muscle organ development 75%, nervous system development 25% in TCs (Fig. 10D) and 50% nervous system development (28%), skeletal system development (27%) muscle organ development (18%) and angiogenesis (18%) and heart development (9%) for FBs (Fig. 13D). The proteins in TCs are attributed to the following *protein classes*: cytoscheletal proteins (30%), structural proteins (17%) and oxidoreductase (13%), signalling molecule (7%), calcium-binding protein (5%) and cell adhesion molecule, cell junction protein, enzyme modulator and transferase (each 4%; Fig. 11A), while in FBs proteins belong to cytoscheletal proteins (18%), cell adhesion molecule (11%), signalling molecule (8%), nucleic acid binding calcium (8%), oxidoreductase (7%), enzyme modulator (7%), receptor (7%; Fig. 14A).

The most significant *pathway* in TCs showed that they are involved mainly in nicotinic acethylcoline receptor signalling pathway (20%), inflammation mediated by chemokine and cytokine (20%) and cytoskeletal regulation by Rho GTPase (20%), *de novo* purine shynthesis (10%), integrin signalling pathway (10%), salvage pyrimidine nucleotides (10%) and Alzheimer disease-presenilin pathways (10%; Fig. 11B). By comparison, FBs proteome clearly depicts that they are involved in synthesizing the extracellular matrix components: integrin signalling pathway (15%), cytoskeletal regulation by Rho GTPase, glycolysis, gonadotropin releasing hormone pathway and Huntington disease (each 10%; Fig. 14B).

The *cellular localization* of TCs proteome demonstrated proteins from cytoscheleton (87%) and plasma membrane (13%; Fig. 11C). In FBs, 76% of the proteins belong to the cytoskeleton, 18% to the extracellular matrix and 6% to the plasma membrane (Fig. 14C).

The heat map showing the expression of differentially expressed protein between TCs and FBs is showed in Figure 15 and demonstrated that the differences between this two cell types are still maintained in cell culture after 10 days.

The main *developmental processes* which employ TCs proteins are anatomical structure morphogenesis (44%) and ectoderm development (32%) mesoderm and system development (each 12%; Fig. 10B), comparative to FBs where anatomical structure morphogenesis, ectoderm development and system development are in equal proportion ~27% each and mesoderm development (19.2%; Fig. 13B).

The *cellular processes* which engage TCs proteins are cellular component organization (34%), cell communication (22%), cell

**Fig. 13** Pie chart representation of the distribution of identified proteins in FBs (cell culture, 10th day) according to their biological processes (**A**), cellular processes (**B**), developmental processes (**C**) and system development (**D**) involvement.

As presented by radar representation both cell types, TCs and FBs suffer a slight switch in phenotype between the 5th and 10th day, however Figures 16A, B and 17A, B clearly show major differences between TCs and FBs.

# Discussion

The domain of proteomics enables comparative analysis of existing proteins in different cells [49]. In addition, it allows monitoring the changes in protein expression during the dynamic transformations that cells undergo during their differentiation [50]. For this reason, we performed a proteomic analysis of TCs compared to FBs, at different time-points (the 5th and 10th day in primary cell culture), to verify if these cells are different from one another and if there are any changes in their differentiation (phenotype) over time. After the identification of targeted proteins, we characterized and associated them with protein families using PANTHER database and analysed them from the functional point of view.

We identified a panel of 1609 proteins from human lung TCs and FBs cell cultures samples which were quantified and the highest fold change expressed proteins between TCs and FBs were analysed and classified using the protein database. According to our results, there were top 39 ranked proteins over expressed in TCs compared to FBs at 5th day in cell culture and 24 up-regulated proteins in TCs by comparison to FBs at 10th day in cell culture and this supports the case for TCs as distinctive cells.

## Putative roles of differentially expressed proteins in TCs

In TCs, by comparison with FBs, the differentially identified proteins were mainly located in the cytoplasmic compartment and involved in cell signalling, energy and metabolic pathways, while a significant part of the FBs proteins were destined to the extracellular matrix which is in concordance with its well known function of producing extracellular matrix components (including collagen) [51].
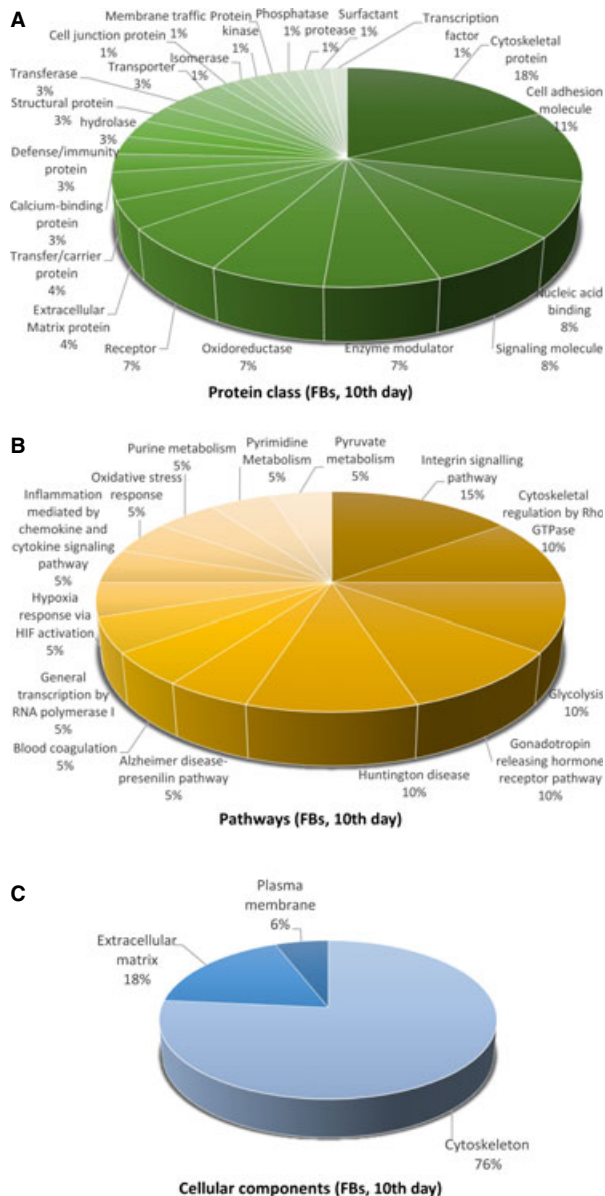
**Fig. 14** Pie chart representation of the distribution of identified proteins in FBs (cell culture, 10th day) according to their protein class (**A**), pathways (**B**) and cellular components (**C**) classifications.

**Myosin-14**, which was found to be up-regulated in TCs, is a conventional non-muscle myosin encoded by the MYH14 gene in human chromosome 19q13.3 [52]. We found that non-muscle myosin-14 seems to be involved in processes such as *sensory perception*, *intercellular signalling* and *morphogenesis*, according to the PANTHER classification system. Among previous assumptions on TCs functions it has been included that of mechanoreceptors [53], capable of detecting and translate stretch information to the nucleus [12, 16]. The presence of cytoskeleton proteins and especially myosin-14 in

TCs confirms this hypothesis. Taking into account that myosin-14 is known to be involved in sensory perception [54], we can propose TCs as candidates for a *mechanical sensing and mechanochemical conversion task*. In addition, the presence of TC primary cilia was reported in vasculature [55] and trachea [56], functioning as mechano- or chemosensors [57], probably involved in the initiation of cellular global positioning to initiate tissue renewal after damage [58].

Telocyte proteome also revealed the presence of periplakin. **Periplakin**, a protein which in humans is encoded by the PPL gene, links cytoskeleton elements together and connects them to junctional complexes [59]. Up till now, electron microscopy studies revealed that TCs establish *homocellular (TC–TC junctions) and heterocellular junctions (TC-other cell type)* [25, 26]. Mechanical junctions are essential to the proliferation, migration and transformation of various cell types [60, 61] and therefore we might suggest that TCs are involved in these mentioned processes. Also, *intercellular signalling* is pivotal in switching cells between different fates such as growth, differentiation and motility, and it could be influenced by tensional force generation within the cytoskeleton [62, 63]. We suggest that TCs might participate in *mechanical sensing and mechanochemical conversion task* and also in *tissue repair/remodelling/renewal*, as shown before [38, 39, 64, 65].

Telocytes proteomic analysis revealed the up-regulation of proteins with oxidoreductase activity, mostly located within mitocondria. It had been proved under electron microscope that TCs have calcium uptake/release units defined by a close relation between caveolae, endoplasmic reticulum and mithocondria [66], located in the podoms of telopodes [12, 16, 26]. It is well known that mitochondria and endoplasmic reticulum establish bilateral physiological interactions responsible (among numerous functions) for modulating the calcium signalling function, process which involves redox and redoxsensitive enzymes [67]. ER–mitochondria crosstalk is essential for eukaryotic cells preventing the onset of diseases by disrupted metabolism [68, 69]. Moreover, Haines *et al.* suggested that the intensity of oxidative stress influences cell tissue composition towards desired cell type ratio, functioning as a cell death 'rheostat' [70]. Therefore, we consider that *TCs are involved in the maintenance of cell and tissue homoeostasis*.

Mammalian cells release extracellular vesicles produced by two mechanisms: (a) secretion from the endosomal membrane compartment after the fusion of multivesicular bodies with a plasma membrane and (b) shedding directly from plasma membrane [71]. Telocytes are no exception to this, the presence of *exosomes and ectosomes* being recently reported [7, 16, 26]. *Several proteins up-regulated in TCs were found among the top 100 vesicular proteins that are present most frequently in mammalian extracellular vesicles proteome* [72]. Among them we can exemplify with proteins such as: mitochondrial thioredoxin-dependent peroxide reductase, protein disulphide-isomerase A3, myosin-14, myosin-10, filamin-B, sodium/potassium-transporting ATPase subunit $\alpha$-1 and keratin, type II cytoskeletal 1. We can assume that the release of extracellular proteins contributes to the extracellular environment homoeostasis, possibly influencing stem cell niches, leading to cell differentiation which is in congruence with very recent studies pointing out that TCs could function as an extensive intercellular information transmission system [73].
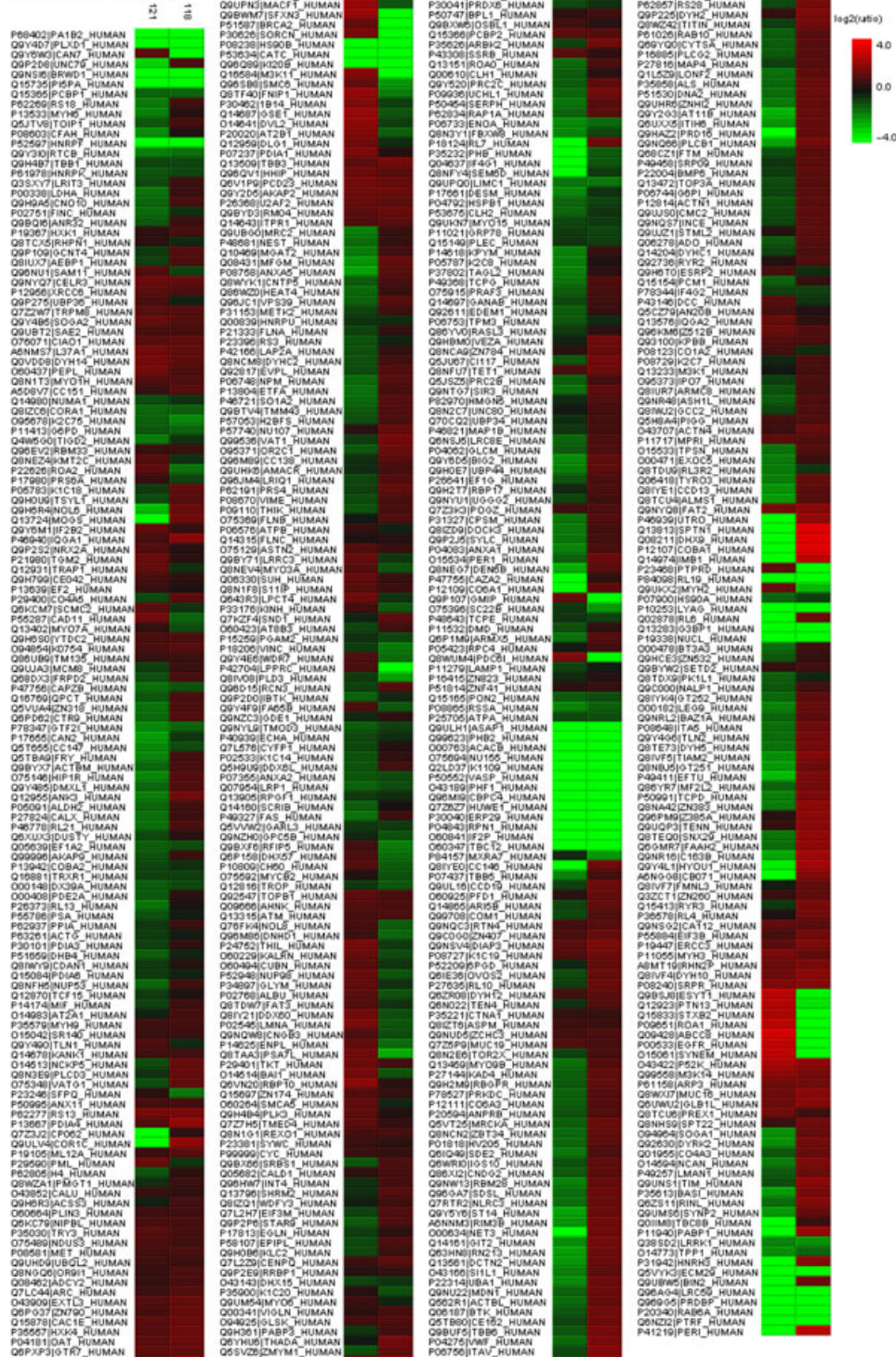
**Fig. 15** Heat map depicting significance results between TCs and FBs (cell culture, 10th day). Experimental samples are clustered on the horizontal axis and protein spots on the vertical axis. Red indicates increased and green decreased expression ratio, while black squares indicate no change in protein abundance. The colour gradient indicates the magnitude of fold change.
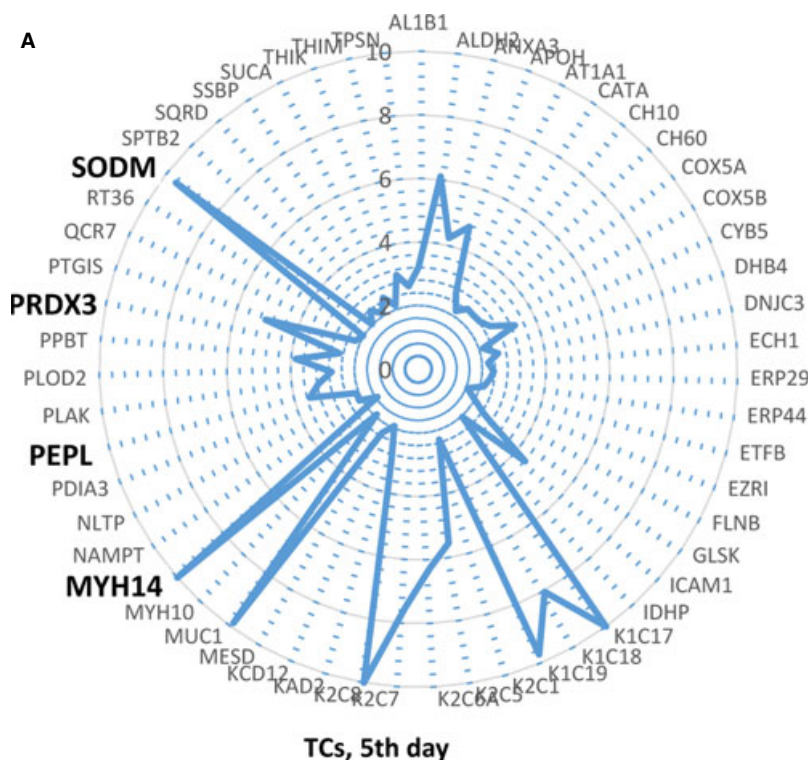
**Fig. 16** (**A–B**) Radars of differential protein expression at 5th day in cell culture for top proteins of TCs (**A**) and FBs (**B**). For display purposes, high values of fold change was limited to 10 in A and to 5 in B, respectively. For proteins with fold change greater than 2, the corresponding fold change value was taken into account, even if lower than 2.

**A**

TCs, 10th day

**B**

FBs, 10th day
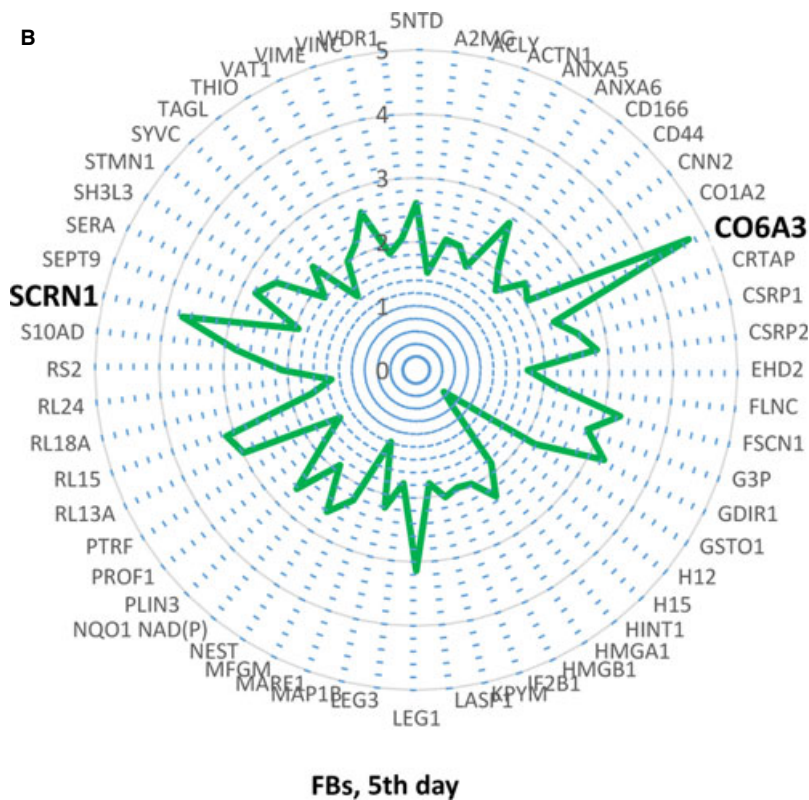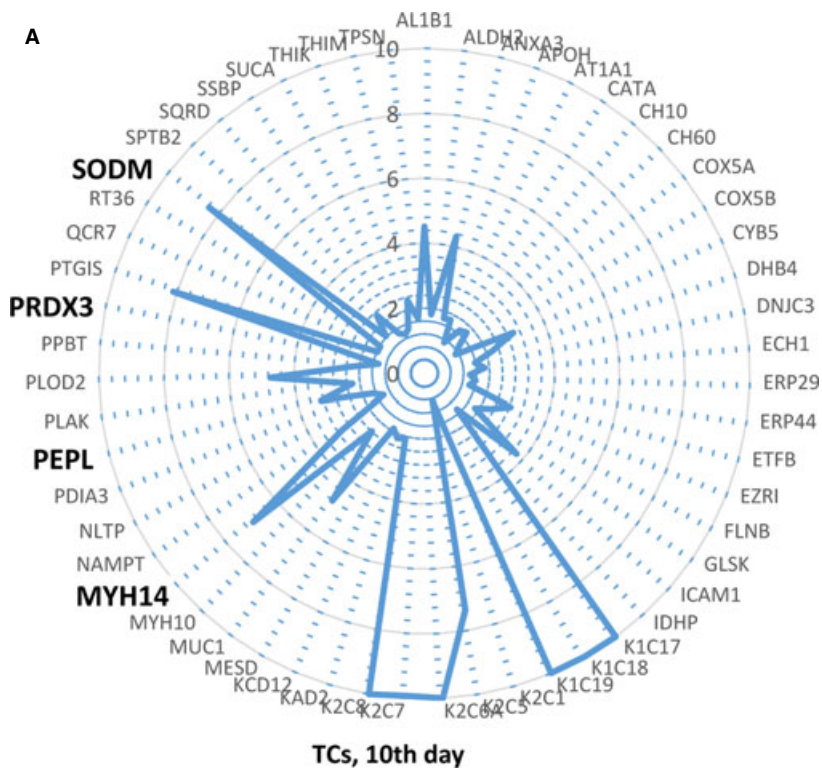
**Fig. 17** (**A**, **B**) Radars of differential protein expression at 10th day in cell culture for top proteins of TCs (**A**) and FBs (**B**). For display purposes, high values of fold change was limited to 10 in **A** and to 5 in **B**, respectively. For proteins with fold change greater than 2, the corresponding fold change value was taken into account, even if lower than 2.
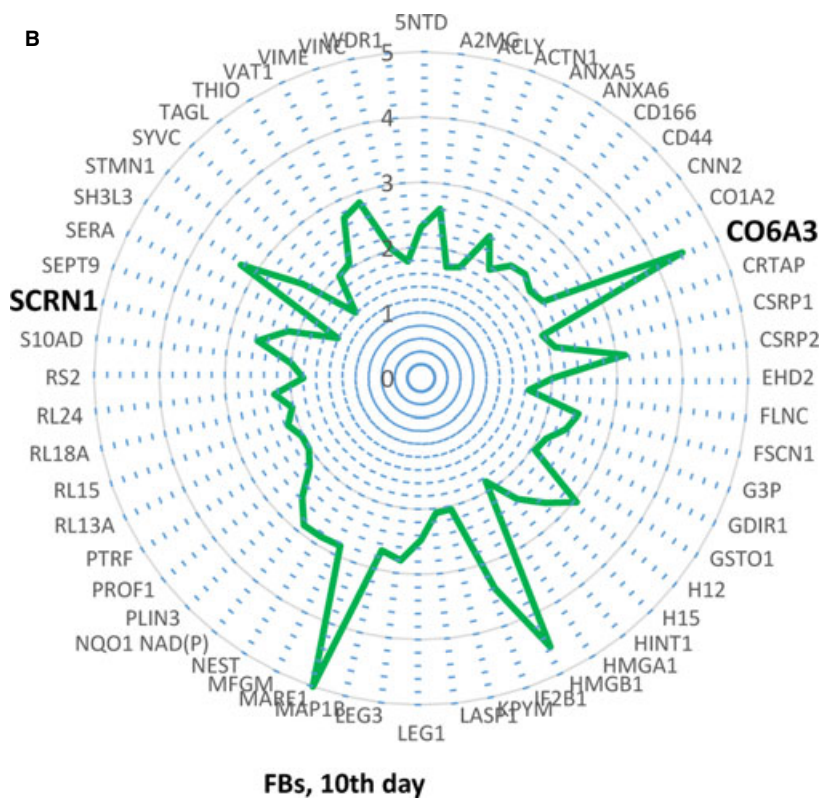
## Conclusion

The present study represents the first proteomic analysis on TCs and will provide useful insights on the possible functions of these cells and involvement in lung (and not only) pathology. The data herein reported show that TCs are completely different from FBs, not only by their ultrastructural configuration [1, 23], gene profile [42], immunophenotype [74], but also from the protein expression point of view. The data presented now are supporting for our previous assumptions regarding TCs functions in tissue morphogenesis, development and repair/remodelling, extracellular environment homoeostasis and intercellular signalling influencing stem cell niche fate.

## Acknowledgements

## Conflicts of interest

The authors confirm that there are no conflicts of interest.

## Supporting information

Additional Supporting Information may be found in the online version of this article:

**Table S1.** Summary of up-regulated TCs proteins (more than two-fold) *versus* FBs 5th day.

**Table S2.** Summary of up-regulated FBs proteins (more than two-fold) *versus* TCs 5th day.

**Table S3.** Summary of up-regulated TCs proteins (more than two-fold) *versus* FBs 10th day.

**Table S4.** Summary of up-regulated FBs proteins (more than two-fold) *versus* TCs 10th day.

## References

1. **Popescu LM, Faussone-Pellegrini MS.** TELOCYTES - a case of serendipity: the winding way from Interstitial Cells of Cajal (ICC), *via* Interstitial Cajal-Like Cells (ICLC) to TELOCYTES. *J Cell Mol Med*. 2010; 14: 729–40.

2. **Popescu LM, Manole CG, Gherghiceanu M, *et al.*** Telocytes in human epicardium. *J Cell Mol Med*. 2010; 14: 2085–93.

3. **Suciu L, Popescu LM, Gherghiceanu M, *et al.*** Telocytes in human term placenta: morphology and phenotype. *Cells Tissues Organs*. 2010; 192: 325–39.

4. **Hinescu ME, Gherghiceanu M, Suciu L, *et al.*** Telocytes in pleura: two- and three-dimensional imaging by transmission electron microscopy. *Cell Tissue Res*. 2011; 343: 389–97.

5. **Manole CG, Cismasiu V, Gherghiceanu M, *et al.*** Experimental acute myocardial infarction: telocytes involvement in neo-angiogenesis. *J Cell Mol Med*. 2011; 15: 2284–96.

6. **Popescu LM, Manole E, Serboiu CS, *et al.*** Identification of telocytes in skeletal muscle interstitium: implication for muscle regeneration. *J Cell Mol Med*. 2011; 15: 1379–92.

7. **Nicolescu MI, Popescu LM.** Telocytes in the interstitium of human exocrine pancreas: ultrastructural evidence. *Pancreas*. 2012; 41: 949–56.

8. **Rusu MC, Pop F, Hostiuc S, *et al.*** Telocytes form networks in normal cardiac tissues. *Histol Histopathol*. 2012; 27: 807–16.

9. **Nicolescu MI, Bucur A, Dinca O, *et al.*** Telocytes in parotid glands. *Anat Rec (Hoboken)*. 2012; 295: 378–85.

10. **Popescu BO, Gherghiceanu M, Kostin S, *et al.*** Telocytes in meninges and choroid plexus. *Neurosci Lett*. 2012; 516: 265–9.

11. **Ceafalan L, Gherghiceanu M, Popescu LM, *et al.*** Telocytes in human skin–are they involved in skin regeneration? *J Cell Mol Med*. 2012; 16: 1405–20.

12. **Cretoiu D, Cretoiu SM, Simionescu AA, *et al.*** Telocytes, a distinct type of cell among the stromal cells present in the lamina propria of jejunum. *Histol Histopathol*. 2012; 27: 1067–78.

13. **Zheng Y, Zhu T, Lin M, *et al.*** Telocytes in the urinary system. *J Transl Med*. 2012; 10: 188.

14. **Qi G, Lin M, Xu M, *et al.*** Telocytes in the human kidney cortex. *J Cell Mol Med*. 2012; 16: 3116–22.

15. **Corradi LS, Jesus MM, Fochi RA, *et al.*** Structural and ultrastructural evidence for telocytes in prostate stroma. *J Cell Mol Med*. 2013; 17: 398–406.

16. **Cretoiu SM, Cretoiu D, Marin A, *et al.*** Telocytes: ultrastructural, immunohistochemical and electrophysiological characteristics in human myometrium. *Reproduction*. 2013; 145: 357–70.

17. **Diaz-Flores L, Gutierrez R, Saez FJ, *et al.*** Telocytes in neuromuscular spindles. *J Cell Mol Med*. 2013; 17: 457–65.

18. **Bosco C, Diaz E, Gutierrez R, *et al.*** Ganglionar nervous cells and telocytes in the pancreas of Octodon degus: extra and intrapancreatic ganglionar cells and telocytes in the degus. *Auton Neurosci*. 2013; 177: 224–30.

19. **Luesma MJ, Gherghiceanu M, Popescu LM.** Telocytes and stem cells in limbus and uvea of mouse eye. *J Cell Mol Med*. 2013; 17: 1016–24.

20. **Chen X, Zheng Y, Manole CG, *et al.*** Telocytes in human oesophagus. *J Cell Mol Med*. 2013; 17: 1506–12.

21. **Xiao J, Wang F, Liu Z, *et al.*** Telocytes in liver: electron microscopic and immunofluorescent evidence. *J Cell Mol Med*. 2013; 17: 1537–42.

22. **Zheng Y, Li H, Manole CG, *et al.*** Telocytes in trachea and lungs. *J Cell Mol Med*. 2011; 15: 2262–8.

23. **Popescu LM, Gherghiceanu M, Suciu LC, *et al.*** Telocytes and putative stem cells in the lungs: electron microscopy, electron tomography and laser scanning microscopy. *Cell Tissue Res*. 2011; 345: 391–403.

© 2014 The Authors.

Journal of Cellular and Molecular Medicine published by John Wiley & Sons Ltd and Foundation for Cellular and Molecular Medicine.

587

24. **Zheng YBC, Wang X.** Telocyte morphologies and potential roles in diseases. *J Cell Physiol.* 2012; 227: 2311–7.

25. **Gherghiceanu M, Popescu LM.** Cardiac telocytes - their junctions and functional implications. *Cell Tissue Res.* 2012; 348: 265–79.

26. **Cretoiu SM, Cretoiu D, Popescu LM.** Human myometrium - the ultrastructural 3D network of telocytes. *J Cell Mol Med.* 2012; 16: 2844–9.

27. **Popescu LM, Gherghiceanu M, Cretoiu D, et al.** The connective connection: interstitial cells of Cajal (ICC) and ICC-like cells establish synapses with immunoreactive cells. Electron microscope study *in situ. J Cell Mol Med.* 2005; 9: 714–30.

28. **Popescu LM, Gherghiceanu M, Kostin S, et al.** Telocytes and heart renewing. In: Wang P, Kuo CH, Takeda N, Singal PK, editors. *Adaptation biology and medicine.* New Delhi: Narosa Publishing House Pvt. Ltd.; 2011. pp. 17–39.

29. **Zhao B, Chen S, Liu J, et al.** Cardiac telocytes were decreased during myocardial infarction and their therapeutic effects for ischaemic heart in rat. *J Cell Mol Med.* 2013; 17: 123–33.

30. **Cretoiu SM, Cretoiu D, Simionescu AA, et al.** Telocytes in human fallopian tube and uterus express estrogen and progesterone receptors. In: Kahn S, editor. *Sex steroids.* Rijeka, Croatia: Intech, 2012. pp. 91–114.

31. **Popescu LM, Nicolescu MI.** Telocytes and stem cells. In: dos Santos Goldenberg RC, Campos de Carvalho AC, editors. *Resident stem cells and regenerative therapy.* Oxford: Academic Press; 2013. pp. 205–31.

32. **Cismasiu VB, Radu E, Popescu LM.** miR-193 expression differentiates telocytes from other stromal cells. *J Cell Mol Med.* 2011; 15: 1071–4.

33. **Sheng J, Shim W, Lu J, et al.** Electrophysiology of human cardiac atrial and ventricular telocytes. *J Cell Mol Med.* 2014; 18: 355–62.

34. **Bani D, Nistri S.** New insights into the morphogenic role of stromal cells and their relevance for regenerative medicine. Lessons from the heart. *J Cell Mol Med.* 2014 Mar; 18(3): 363–70.

35. **Vannucchi MG, Traini C, Manetti M, et al.** Telocytes express PDGFRalpha in the human gastrointestinal tract. *J Cell Mol Med.* 2013; 17: 1099–108.

36. **Zhao B, Liao Z, Chen S, et al.** Intramyocardial transplantation of cardiac telocytes decreases myocardial infarction and improves post-infarcted cardiac function in rats. *J Cell Mol Med.* 2014; 18. (in press). Doi:10.1111/jcmm.12259.

37. **Milia AF, Ruffo M, Manetti M, et al.** Telocytes in Crohn's disease. *J Cell Mol Med.* 2013; 17: 1525–36.

38. **Manetti M, Guiducci S, Ruffo M, et al.** Evidence for progressive reduction and loss of telocytes in the dermal cellular network of systemic sclerosis. *J Cell Mol Med.* 2013; 17: 482–96.

39. **Manetti M, Rosa I, Messerini L, et al.** A loss of telocytes accompanies fibrosis of multiple organs in systemic sclerosis. *J Cell Mol Med.* 2014; 18: 253–62.

40. **Matyja A, Gil K, Pasternak A, et al.** Telocytes: new insight into the pathogenesis of gallstone disease. *J Cell Mol Med.* 2013; 17: 734–42.

41. **Mou Y, Wang Y, Li J, et al.** Immunohistochemical characterization and functional identification of mammary gland telocytes in the self-assembly of reconstituted breast cancer tissue *in vitro. J Cell Mol Med.* 2013; 17: 65–75.

42. **Zheng Y, Zhang M, Qian M, et al.** Genetic comparison of mouse lung telocytes with mesenchymal stem cells and fibroblasts. *J Cell Mol Med.* 2013; 17: 567–77.

43. **Wright JC, Hubbard SJ.** Recent developments in proteome informatics for mass spectrometry analysis. *Comb Chem High Throughput Screen.* 2009; 12: 194–202.

44. **Cox J, Michalski A, Mann M.** Software lock mass by two-dimensional minimization of peptide mass errors. *J Am Soc Mass Spectrom.* 2011; 22: 1373–80.

45. **Wang JG, Xu WD, Zhai WT, et al.** Disorders in angiogenesis and redox pathways are main factors contributing to the progression of rheumatoid arthritis: a comparative proteomics study. *Arthritis Rheum.* 2012; 64: 993–1004.

46. **Jin GZ, Li Y, Cong WM, et al.** iTRAQ-2DLC-ESI-MS/MS based identification of a new set of immunohistochemical biomarkers for classification of dysplastic nodules and small hepatocellular carcinoma. *J Proteome Res.* 2011; 10: 3418–28.

47. **Gilar M, Olivova P, Daly AE, et al.** Two-dimensional separation of peptides using RP-RP-HPLC system with different pH in first and second separation dimensions. *J Sep Sci.* 2005; 28: 1694–703.

48. **Mi H, Muruganujan A, Casagrande JT, et al.** Large-scale gene function analysis with the PANTHER classification system. *Nat Protoc.* 2013; 8: 1551–66.

49. **Navarro P, Trevisan-Herraz M, Bonzon-Kulichenko E, et al.** General statistical framework for quantitative proteomics by stable isotope labeling. *J Proteome Res.* 2014; 13: 1234–47.

50. **Shim JH, Cho SA, Seo MJ, et al.** Proteomic analysis of time-dependent difference of protein expression profile changes during neuronal differentiation of mouse embryonic stem cells. *Mol Cells.* 2010; 29: 239–44.

51. **Abonnenc M, Nabeebaccus AA, Mayr U, et al.** Extracellular matrix secretion by cardiac fibroblasts: role of microRNA-29b and microRNA-30c. *Circ Res.* 2013; 113: 1138–47.

52. **Leal A, Endele S, Stengel C, et al.** A novel myosin heavy chain gene in human chromosome 19q13.3. *Gene.* 2003; 312: 165–71.

53. **Hinescu ME, Popescu LM, Gherghiceanu M, et al.** Interstitial Cajal-like cells in rat mesentery: an ultrastructural and immunohistochemical approach. *J Cell Mol Med.* 2008; 12: 260–70.

54. **Zong L, Lu C, Zhao Y, et al.** Clue to a new deafness gene: a large Chinese nonsyndromic hearing loss family linked to DFNA4. *J Genet Genomics.* 2012; 39: 653–7.

55. **Cantarero I, Luesma MJ, Junquera C.** The primary cilium of telocytes in the vasculature: electron microscope imaging. *J Cell Mol Med.* 2011; 15: 2594–600.

56. **Rusu MC, Jianu AM, Mirancea N, et al.** Tracheal telocytes. *J Cell Mol Med.* 2012; 16: 401–5.

57. **Castiella T, Munoz G, Luesma MJ, et al.** Primary cilia in gastric gastrointestinal stromal tumours (GISTs): an ultrastructural study. *J Cell Mol Med.* 2013; 17: 844–53.

58. **Clement CA, Ajbro KD, Koefoed K, et al.** TGF-beta signaling is associated with endocytosis at the pocket region of the primary cilium. *Cell Rep.* 2013; 3: 1806–14.

59. **Leung CL, Green KJ, Liem RK.** Plakins: a family of versatile cytolinker proteins. *Trends Cell Biol.* 2002; 12: 37–45.

60. **Menko AS, Bleaken BM, Walker JL.** Regional-specific alterations in cell-cell junctions, cytoskeletal networks and myosin-mediated mechanical cues coordinate collectivity of movement of epithelial cells in response to injury. *Exp Cell Res.* 2014; 322: 133–48.

61. **Asimaki A, Saffitz JE.** Remodeling of cell-cell junctions in arrhythmogenic cardiomyopathy. *Cell Commun Adhes.* 2014; 21: 13–23.

62. **Mammoto T, Mammoto A, Ingber DE.** Mechanobiology and developmental control. *Annu Rev Cell Dev Biol.* 2013; 29: 27–61.

63. **Planas-Paz L, Lammert E.** Mechanosensing in developing lymphatic vessels. *Adv Anat Embryol Cell Biol.* 2014; 214: 23–40.

64. **Popescu LM, Gherghiceanu M, Manole CG, et al.** Cardiac renewing: interstitial Cajal-like cells nurse cardiomyocyte progenitors in

epicardial stem cell niches. *J Cell Mol Med*. 2009; 13: 866–86.

65. **Zhou J, Wang Y, Zhu P, *et al.*** Distribution and characteristics of telocytes as nurse cells in the architectural organization of engineered heart tissues. *Sci China Life Sci*. 2014; 57: 241–7.

66. **Popescu LM, Gherghiceanu M, Mandache E, *et al.*** Caveolae in smooth muscles: nanocontacts. *J Cell Mol Med*. 2006; 10: 960–90.

67. **Csordas G, Renken C, Varnai P, *et al.*** Structural and functional features and significance of the physical linkage between ER and mitochondria. *J Cell Biol*. 2006; 174: 915–21.

68. **Kopach O, Kruglikov I, Pivneva T, *et al.*** Functional coupling between ryanodine receptors, mitochondria and Ca(2 + ) ATPases in rat submandibular acinar cells. *Cell Calcium*. 2008; 43: 469–81.

69. **Raturi A, Simmen T.** Where the endoplasmic reticulum and the mitochondrion tie the knot: the mitochondria-associated membrane (MAM). *Biochim Biophys Acta*. 2013; 1833: 213–24.

70. **Haines DD, Juhasz B, Tosaki A.** Management of multicellular senescence and oxidative stress. *J Cell Mol Med*. 2013; 17: 936–57.

71. **Gyorgy B, Szabo TG, Pasztoi M, *et al.*** Membrane vesicles, current state-of-the-art: emerging role of extracellular vesicles. *Cell Mol Life Sci*. 2011; 68: 2667–88.

72. **Choi DS, Kim DK, Kim YK, *et al.*** Proteomics of extracellular vesicles: exosomes and ectosomes. *Mass Spectrom Rev*. 2014. (in press). Doi:10.1002/mas.21420.

73. **Smythies J, Edelstein L.** Telocytes, exosomes, gap junctions and the cytoskeleton: the makings of a primitive nervous system? *Front Cell Neurosci*. 2014; 7: 278.

74. **Galiger C, Kostin S, Golec A, *et al.*** Phenotypical and ultrastructural features of Oct4-positive cells in the adult mouse lung. *J Cell Mol Med*. 2014 doi: 10.1111/jcmm.12295